PCCP

Accepted Manuscript

ROYAL SOCIETY OF CHEMISTRY

www.rsc.org/pccp

A Slowing Down of Proton Motion from HPTS to Water Adsorbed on MCM-41 Surface

Noemí Alarcos, Boiko Cohen and Abderrazzak Douhal*

Departamento de Química Física, Facultad de Ciencias Ambientales y Bioquímica, and INAMOL, Universidad de Castilla-La Mancha, Avenida Carlos III, S.N., 45071 Toledo, Spain.

*Corresponding author at Universidad de Castilla-La Mancha.

Tel.: +34 925 265717; E-mail address: abderrazzak.douhal@uclm.es

Abstract

We report on the steady-state and femtosecond-nanosecond (fs-ns) behaviour of 8-hydroxypyrene-1,3,6-trisulfonate (pyranine, HPTS) and its interaction with mesoporous silica based materials (MCM-41) in both solid-state and dichloromethane (DCM) suspensions in absence and presence of water. In absence of water, HPTS forms aggregates which are characterized by show a broad emission spectrum and a multiexponential behavior ($\tau_{solid\text{-}state/DCM}$ = 120 ps, 600 ps, 2.2 ns). Upon interaction with MCM41, the aggregates population is lower, leading to the formation of adsorbed monomers. In presence of water (1%), HPTS with and without MCM41 materials in DCM suspensions, undergoes an excited-state intermolecular proton-transfer (ESPT) reaction in the protonated forms (ROH*) producing the deprotonated species (RO^-*). The long-time emission decays of the ROH* in the different systems in presence of water are multiexponential, and are analysed using the diffusion-assisted geminate recombination model. The obtained proton-transfer and recombination rate constants for HPTS and HPTS/MCM41 complexes in DCM suspensions in presence of water are k_{PT} = 13 ns^{-1}, k_{rec} = 7.5 Å/ns, and k_{PT} = 5.4 ns^{-1}, k_{rec} = 2.2 Å/ns, respectively, The slowing down of both processes in the latter case, is explained in terms of specific interactions of the dye and of the water molecules with the silica surface. The ultrafast dynamics (fs-regime) of the HPTS/MCM41 complexes in DCM suspensions, without and with water, shows two components which are assigned to intramolecular vibrational-energy relaxation (IVR) (~120 fs vs ~0.8 ps), and vibrational relaxation/cooling (VC), and charge transfer (CT) processes (~2 ps without water and ~5 ps with water) of the adsorbed ROH*. Our results provide new knowledge on the interactions and the proton-transfer reaction dynamics of HPTS adsorbed on mesoporous materials.

Keywords: mesoporous materials, photoacid, intermolecular proton transfer, femtosecond dynamics, solvation, recombination, surface femtochemistry.

1. Introduction

The interaction of molecules with solid supports is of fundamental interest for many research fields, ranging from biology, chemistry, physics to nanotechnology.[1-8] These interactions and the resulting hybrid complexes have multiple implications for the development of new technological processes, such as photonic devices, drug delivery platforms or catalysis.[9-13] In the latter, the development of solid supports based on silica materials such as MCM-41 or zeolites has drawn much attention in recent years.[11, 14, 15]

Aromatic acids are a special class of compounds that upon excitation become strong acids capable to undergo an excited-state intermolecular proton-transfer (ESPT) reaction with the neighbouring molecule (water or base).[16-23] A well-known example is pyranine (8-hydroxypyrene-1,3,6-trisulfonated, HPTS) (Scheme 1).[19, 24-29] In aqueous solutions, the overall ESPT reaction is subdivided into two main consecutive physico-chemical events (initial proton transfer and recombination of the ion pair) followed by a diffusive motion of the proton around the deprotonated (RO^-) species. The latter process is described by the Debye-Smoluchowski equation (DSE) (Scheme 1).[30] In the last decade, picosecond, femtosecond fluorescence up-conversion and pump-probe studies have revealed the related dynamics.[25, 29, 31, 32] These reports have found that the initial dynamics of HPTS involves two ultrafast steps (300 fs and 3 ps), which precede the proton-transfer step (~100 ps). The 300 fs and 3 ps have been assigned to vibrational relaxation (VR) and local excited (LE) to charge transfer (CT) conversion in the excited enol form (ROH).[28, 32]

When HPTS is confined within chemical or biological cavities, changes in its photodynamics were observed.[33-37] In γ-CD compared to water situation, a slowing down of the initial proton transfer step (k_{PT} = 4 ns^{-1} vs k_{PT} = 10 ns^{-1}) and the recombination process (k_{rec} = 2.2 Å/ns vs k_{rec} = 6 Å/ns) is observed.[36, 37] Other behaviour was observed in reverse micelles where the recombination process was faster than in water (k_{rec} = 8.6 Å/ns (for radius size 7 Å) vs k_{rec} = 6 Å/ns) while that of dissociation was slower (k_{PT} = 7.5 ns^{-1} (for radius size 7 Å) vs k_{PT} = 10 ns^{-1}).[33] The encapsulation of HPTS in a supramolecular assembly consisting of a triblock copolymer and a cationic surfactant also shows similar results.[35] In the human serum albumin (HSA) protein, reversible and direct proton transfer reactions were observed.[34] The reversible ESPT that takes place between HPTS and the biological water present in the HSA cavity exhibits a slowing down due to the confinement effect on water dynamics, a behaviour

similar to the one observed using γ-CD.[34] On the other hand, the direct ESPT reaction has an ultrafast time component of 150 fs and involves the carboxylate groups of the amino acids.[34] HPTS covalently linked to both hydrophilic alumina and silica surface, and HPTS confined in silicon pores (10 nm of diameter), showed that the ESPT dynamics was similar to that in bulk water.[38, 39] In the first case, HPTS retains its photoacid properties despite being covalently linked through a sulfonate group.[38] In the second one, the size of the pores is too large that HPTS does not experience a confinement effect.[39] Thus, additional studies are needed to fully understand the interaction of HPTS with silica-based material and how such interactions affect not only the slow ESPT reaction with absorbed water on its surface, but also the initial ultrafast dynamics of the system.

Here, we report on the steady-state and femtosecond-nanosecond (fs-ns) behaviour of HPTS and HPTS interacting with MCM-41 in both solid-state and DCM suspensions. In solid state, the presence of aggregates, as result of π-π interactions dictates its spectroscopy and dynamics. The interaction with MCM-41 decreases the aggregates population, and thus that of interacting protonated monomers (ROH) increases. Because of similar results using silica particles and MCM-41, we suggest that that HPTS is interacting predominantly with the external MCM-41 surface. HPTS and HPTS/MCM-41 composites were also suspended in dichloromethane (DCM) solution containing μL of water. A reversible excited-state proton-transfer (ESPT) reaction between HPTS and the added water molecules takes place. Due to the observed recombination process, the emission data are analysed by the geminate recombination (GR) model (SSDP program). For HPTS in DCM suspensions containing water, the values of proton-transfer and recombination rate constants, k_{PT} (13 ns^{-1}) and k_{rec} (7.5 Å/ns), respectively, are higher than those obtained in bulk water (k_{PT} (10 ns^{-1}) and k_{rec} (6 Å/ns)).[31, 37] However, for HPTS/MCM-41 complexes, the presence of water leads to a slower dynamics (k_{PT} = 5.4 ns^{-1} and k_{rec} = 2.2 Å/ns) due to the specific interactions with the MCM-41surface. In this complex, the kinetic isotope effect (KIE) for the dissociation process (k^H_{PT}/k^D_{PT}) is 2, while for the recombination one, (k^H_{rec}/k^D_{rec}) it is 1.3. Finally, the fs-studies of the HPTS/MCM-41 in DCM suspensions, in absence and in presence of water, show stronger interactions between HPTS and the MCM-41 surface. In absence of water, we found two time constants of ~120 fs and ~2 ps; while in presence of water, these time constants are ~0.8 ps and 5 ps. The shorter component is assigned to the intramolecular vibrational-energy redistribution (IVR), while the

longer one is a combination of vibrational cooling (VC) and charge transfer (CT) processes of ROH* forms.

2. Experimental Section

Trisodium 8-hydroxypyrene-1,3,6-trisulfonate (pyranine, HPTS, purity >98%, Fluka), dichloromethane (DCM, spectroscopic grade, 99.9%, Scharlab), deuterium oxide (D_2O, 99.9%, Sigma-Aldrich) and MCM-41 (Mobil Crystalline Material, nº 41) mesoporous material (Sigma Aldrich) were used as received. HPTS/MCM-41 composites were prepared by adding 100 mg of dried MCM-41 to 10 ml of HPTS in a DCM solution (1×10^{-5} M). For the experiment of concentration effect, the concentration of HPTS in the initial DCM solution was 1×10^{-3} M. HPTS/SiO_2 composites were prepared by adding 100 mg of dried SiO_2 to 10 ml of HPTS in a DCM solution (1×10^{-5} M). All suspensions were stirred at room temperature during 24 h. The mixtures were centrifuged and rinsed four times with pure DCM to remove the weakly adsorbed dye molecules. The resulted solids were then dried under vacuum at room temperature.

The steady-state UV-visible diffuse transmittance was recorded using JASCO V-670 spectrophotometer equipped with a 60 mm integrating sphere ISN-723. The obtained signals were converted from Kubelka-Munk function F(R)=((1-R)2)/2R, where R is the diffuse transmittance from the sample. Emission spectra were recorded using Fluoromax-4 (Jobin-Yvone) spectrofluorimeter. Picosecond emission decays were measured using a time-correlated single photon counting (TSCPC) system.[40] For excitation at 350 nm, we used the second harmonic of the output (700 nm, 90 fs, 250 mW, 80 MHz) from a Ti:sapphire oscillator (Mai Tai HP, Spectra Physics). In this experiment, the femtosecond-laser excitation was set at very low power (<0.5 mW) to avoid undesired photochemistry. For excitation at 370 nm, the sample was pumped by a 40-ps pulsed diode laser (<5 mW, 40 MHz). The emission signal was collected at the magic angle and the instrument response function (IRF) was ~40 ps or 70 ps using fs- or ps- pulses excitation, respectively. The IRF of the system has been measured using a standard LUDOX (Sigma-Aldrich) solution in 1 cm cell. The decays were deconvoluted and fitted to a single or multiexponential function using the FLUOFIT package (PicoQuant) allowing single and global fits. The quality of the fit was estimated by χ^2,

which was always below 1.2, and the distribution of the residues. All experiments were done at 293 K. The estimated errors for the obtained values are within 15-20 % range.

The fs-emission transients have been collected using the fluorescence up-conversion technique. The system consists of a fs-Ti:sapphire oscillator (MaiTai HP, Spectra Physics) coupled to a second harmonic generation and up-conversion setup.[41] The oscillator pulses (90 fs, 250 mW, 80 MHz) were centered at 740 nm and doubled in an optical setup through a 0.5-mm BBO crystal to generate a pumping beam at 370 nm (~ 0.1 nJ). The polarization of the latter was set to magic angle with respect to the fundamental gating beam. The sample has been placed in a 1-mm thick rotating cell. The fluorescence was focused with reflective optics into a 1.0-mm BBO crystal and gated with the remaining fundamental fs-beam. The IRF of the full setup (measured as a Raman signal of pure solvent) was 220 fs. To analyse the decays, a multiexponential function convoluted with the IRF was used to fit the experimental transients. All the experiments were performed at 293 K. The estimated error of the obtained values is of 15-20%.

3. Results and Discussion

3.1 Steady-State Observation

3.1.1 Solid-State of HPTS and HPTS/MCM-41

Figure 1 shows the diffuse transmittance (DT) and emission spectra of HPTS (powder) and HPTS interacting with MCM-41 in solid-state. The solid HPTS has a broad and structureless DT spectrum with a maximum around 400 nm (Figure 1A). When HPTS interacts with MCM-41, the spectrum exhibits two well-defined peaks at 378 and 403 nm, in addition to the one at ~300 nm. Similar spectral behaviour has been observed for the protonated form of HPTS (Scheme 1) in methanol (MeOH) and in water solutions, with maxima at 403 and 404 nm, respectively.[34, 42, 43] Previous reports on HPTS confined in γ-CD,[37] human serum albumin (HSA) protein[34] and cetyltrimethyl ammonium bromide (CTAB) micelle[44], showed a similar behaviour. Thus, we assign the DT spectra of both samples (solid HPTS and interacting with MCM-41) to the protonated forms of the dye (ROH, Scheme 1A) at the S_0 state. However, the broad shape of the solid HPTS spectrum indicates the presence of aggregates as a result of π-π interactions, as it has been observed for pyrene, a molecule having the same aromatic

structure, but lacking functional groups,[45, 46] and for other molecules with similar structure and containing sulfonate groups.[47, 48] On the other hand, upon interaction with MCM-41, the aggregates population is strongly reduced.

The emission spectrum of the solid HPTS (Figure 1B) displays a broad band (full width at half maximum (fwhm) = 4100 cm^{-1}) with a maximum at 520 nm, while that of HPTS/MCM-41 shows a relatively narrower band (fwhm = 3180 cm^{-1}) with an intensity maximum at 445 nm. The broad emission spectrum of the solid HPTS can be explained by the formation of different type of aggregates (face-to-face, edge-to-face or end-to-face), and is in agreement with the DT spectrum.[48] Interacting with MCM-41 the monomers are the main emitting species having the emission maximum at 445 nm. This indicates that the interaction with the framework of the mesoporous material suppresses or strongly decreases the formation of aggregates. Similar behaviour was observed for pyrene, where the study of the confinement within mesoporous materials of different pore sizes allowed to distinguish between the emissions of monomers and aggregates.[49]

The fluorescence excitation spectra of solid HPTS and interacting with MCM-41 are well defined, and show narrower bands (more resolved) in comparison with the DT ones (Figures S1A and S1B, respectively, in ESI†). For the HPTS powder, the spectra show two main peaks at 360 and 430 nm. This indicates the presence of two ground-state species in the solid HPTS, which emit in the same region. For the HPTS/MCM-41 composites, the excitation spectra show similar intensity maxima as in the diffuse transmittance spectrum (375 and 404 nm). The intensity tail at 450 nm and that of the peak at 290 nm depend on the observation wavelength indicating the presence of different fluorophores generated from different species at S_0.

3.1.2 HPTS and HPTS/MCM-41 in DCM suspensions with and without water

When solid HPTS is suspended in a DCM solution, it presents a spectral behaviour (Figures S2 in ESI†) similar to the one observed for the solid HPTS (Figure 1). The broad DT spectrum exhibits a broad band with intensity maxima at 300, and 400 nm, while the emission spectrum has its intensity maximum at ~515 nm (Figure S2B in ESI†). The fwhm of the DT and emission spectra (8210 and 3995 cm^{-1}, respectively) are comparable to those obtained for the solid sample (7870 and 4100 cm^{-1}, respectively). These results reflect that HPTS is only slightly affected by the presence of the DCM solvent. However, the spectral behaviour of the HPTS/MCM-41 complexes in DCM

(Figure S2A in ESI†) is different from the corresponding solid sample (Figure 1A). While the DT spectrum exhibits the same bands (290, 378 and 403 nm) and similar fwhm (5535 cm^{-1} vs 5780 cm^{-1} in the solid state), the emission spectrum, whose fwhm (3675 cm^{-1}) also is similar to the one obtained in the solid state (3180 cm^{-1}), has its intensity maximum shifted to shorter wavelengths by ~15 nm (Figure S2B in ESI†). In contrast with the behaviour of the solid HPTS in DCM suspension, the HPTS/MCM-41 one is more affected by the solvent. To know if HPTS is adsorbed on the external surface or confined within its pores, we studied HPTS interacting with silica particles (surface lacking nanopores) where the interactions are on silica surface. The DT and emission spectra (Figure S3A in ESI†) are very similar to those using MCM-41 (Figure S2 in ESI†) suggesting that for HPTS/MCM-41 composites, the dye is most probably adsorbed on the external crystal surface.

To explore the interactions of adsorbed HPTS and water on the MCM-41 surface, we studied the suspensions of solid HPTS and HPTS/MCM-41 in DCM in presence of water. The DT and emission spectra of HPTS in the DCM suspension containing water are comparable to the ones obtained in pure water (Figure S4 in ESI†).[36, 37, 50, 51] Clearly, the presence of water reduces the HPTS aggregates population, and as a result the absorption of the ROH monomers increases. The emission spectrum shows two bands: a band of low intensity at 440 nm and another one of higher intensity at 515 nm (Figure S4B in ESI†). The blue band is assigned to the protonated form (ROH*), while the green one is due to the deprotonated species (RO^-*), in agreement with the band assignment for HPTS in pure water.[36, 37, 50, 51] The relative intensities of ROH* and RO^-* emission depend on water content, being largely reduced the fluorescence of the former at higher water amount (Figure S4B in ESI†).

The HPTS/MCM-41 composite in presence of water shows a spectral behaviour similar to the previous sample (Figure 2). To prove that HPTS is still interacting with MCM-41 after adding water, we studied differently prepared HPTS/MCM-41 complexes where the water has primarily been confined in the MCM-41 before making the complex with HPTS. To prepare hydrated MCM-41 without its collapse, we followed a procedure described elsewhere. [52] We found that the steady-state absorption and emission spectra of these hydrated complexes (Figure S5 in ESI†) are similar to those obtained using dried HPTS/MCM-41 composites in DCM containing water (Figure 2). This suggests that the dye interacts with MCM-41 forming a robust complex

where the water molecules can solvate its molecules attached to the MCM-41 framework and give rise to the ESPT reaction.

3.2. Picosecond Time-Resolved Fluorescence Study

3.2.1 HPTS and HPTS/MCM-41 in Solid-State and DCM suspensions

To get information on the ps behaviour of the different structures present in HPTS and HPTS/MCM-41, we examined their ps-photodynamics in solid-state and in DCM suspensions. Figure 3 shows representative emission decays collected at 450 and 500 nm, following an excitation at 350 nm. The instrumental response function (IRF) is ~40 ps. Table 1 gives the obtained time constants (τ_i), the pre-exponential factors (a_i) and relative contributions (c_i) normalized to 100 after a multiexponential fit, using a global analysis procedure.

The solid HPTS exhibits a multiexponential behaviour with three lifetimes: 120 ps, 600 ps and 2.2 ns. The pre-exponential factor of the 120-ps component increases from 42% at 450 nm to 65% at 600 nm (Table 1). The other components of 600 ps and 2.2 ns, have a maximum contribution toward the shorter wavelengths: 41% at 470 nm and 22% at 450 nm, respectively. The multiexponential character of the emission decays can be explained by the different π-π interactions between the HPTS molecules that lead to formation of different aggregates. Organic salts of anthracene-1,5-disulfonate in crystalline state, form π-stacks with different configurations (face-to-face, edge-to-face and end-to-face) and different packing (slipped column, zigzag column, bricks and herringbone).[48] Each of these interactions results in a multiexponential behaviour.[48] Therefore, we suggest that the three observed components are due to different interactions between the HPTS molecules. Previous reports on the aggregation of HPTS in presence of different organic molecules with cationic character and variable size such as viologen derivatives have shown that in the formed π-stacks, the HPTS molecule is alternated by a cationic one and so the repulsion between the sulfonate groups of the different HPTS molecules was minimized.[53, 54] These observations lead us to suggest that for pure HPTS, and in similarity with the anthracene-1,5-disulfonate case,[47, 48] the sodium cations are probably intercalated between the HPTS molecules giving a stable π-π packing.

When solid HPTS is suspended in DCM a similar photodynamical behaviour is observed with the same emission lifetimes (120 ps, 600 ps and 2.2 ns, Table S1 in

ESI†). This demonstrates that non-interacting solvents, such as DCM, do not affect the excited state behaviour of solid HPTS in agreement with the steady-state results.

The emission decay of the solid HPTS/MCM-41 complex is bi-exponential with lifetimes of 840 ps and 3.9 ns (Figure 3). The first component has the maximum value of the pre-exponential factor at 400 nm (36%), while that of the 3.9-ns one slightly increases towards longer wavelengths (64-67 %, Table 1). As the steady-state results have shown, the interaction with the mesoporous material leads to a strong decrease in the aggregates population, and to an increase in the monomer one, which indicates a strong interaction between MCM-41 and HPTS. The anion emission is not observed, reflecting that no proton-transfer reaction occurs between the mesoporous material and the HPTS molecules. We suggest that both components can be due to decay of different monomer populations of the protonated form (ROH*) with different orientations and interactions of HPTS on the MCM-41 surface (Scheme 2A). However, we cannot entirely exclude the presence of HPTS aggregates on the MCM41 surface. The shortest component may be a combination of different population (monomer and aggregate species) which shows the heterogeneous nature of the hybrid material samples, as observed in other silica-based composites.[7, 55-58] More specifically, a similar behaviour was found in a study of HPTS in dry silicon pores (PSi) where the time-resolved emission signal showed monomers and aggregates presence on the surface.[39]

In presence of DCM (suspension sample), the above components become shorter (2.5 ns and 350 ps, respectively, Table 1B). The presence of the DCM solvent affects HPTS/MCM-41 photodynamics, in agreement with the steady-state experiments. In order to better characterize the sites of interaction between HPTS and MCM-41, we studied HPTS complexed to silica nanoparticles (SiO_2) in DCM (Figure S3 and Table S1 in ESI†). We observed similar behaviour and emission lifetimes (320 ps and 2.3 ns) to that obtained for HPTS/MCM-41. This result is a further evidence that when HPTS is complexed to MCM-41, it mainly interacts through its sulfonate groups (SO_3^-) with the OH-groups of the silica-based surface. Thus, the different orientations of HPTS and the presence of aggregates result in different populations and therefore in a complex photobehaviour. The shortening in the fluorescence lifetimes in suspensions suggests a change in the HPTS/MCM-41 interactions due to the presence of DCM. The increased orbitals coupling between the adsorbed HPTS molecules and the MCM-41 surface, as a result of DCM solvation, can increase the probability of radiationless deactivation pathways.[56, 59, 60]

For a better evaluation of the aggregates contribution in the composites dynamical behavior, we investigated the concentration effect of the dye on the HPTS/MCM-41 complexes. To this end, we studied dye-concentrated samples (HPTS 10^{-3} M/100 mg MCM-41). In this case, the emission spectrum shows an additional new band around ~520 nm (Figure S6A in ESI†). Moreover, we observed a shortening in the fluorescence lifetimes (Figure S6B in ESI†). The decays show two behaviours (Table S1 in ESI†): one from 400 to 510 nm (region I) and another one from 525 to 620 nm (region II). In region I, three components are needed to accurately fit the signal, 50 ps, 320 ps and 2.5 ns. The 320 ps and 2.5 ns components are similar to those observed in less concentrated HPTS/MCM-41 complexes (HPTS 10^{-5} M/100 mg MCM-41). The 50-ps component having the highest contribution (60-48 %).is not observed in the less concentrated composites These results suggest more formation of aggregates on the MCM-41 surface when working at higher dye amounts. Finally, in region II, three components different to the previous ones are observed, giving lifetimes of, 120 ps, 600 ps and 2.2 ns. These values are similar to those observed for HPTS in DCM suspensions (Table S1 in ESI†). Therefore, an increase in the dye concentration within the composites leads to aggregates formation.

3.2.2 HPTS and HPTS/MCM-41 in DCM suspension containing water

Next we studied the picosecond behaviour of HPTS and HPTS/MCM-41 composites in DCM suspensions containing water.

3.2.2.1 HPTS in DCM containing water

To begin with, we briefly discuss the proton-transfer process of HPTS in water, which will serve as a reference. The obtained emission decays are multiexponential in agreement with previous reports.[20, 33, 51, 61-64] Figure S7 shows the obtained fits using two and three exponential functions along with the calculated residuals, and giving χ^2 of 5.75 and 1.10, respectively. We found that three components of 90 ps (present as a decay and rise in the blue and red parts of the emission spectrum, respectively), 720 ps and 5 ns (Table 2) are necessary to get a good fit (Figure 4 and Figure S7 in ESI†). Following previous reports,[31, 32, 35, 50, 62, 65] the shorter component can be assigned to the proton-transfer process, and the longer one to the lifetime of the excited deprotonated

structure (RO^-*). The intermediate component and the multiexponential dynamics are a clear evidence for the presence of geminate recombination (GR).[63] In water, the excited state dynamics of HPTS is adequately described by a reversible ESPT reaction mechanism, where after the formation and the recombination (back reaction) of the ion-pair, (RO^----H_3O^+)*, the probability of finding the ion-pair at a distance "r", and at a time t, is given by the transient numerical solution of the Debye-Smoluchowski equation (DSE) (Scheme 1B).[19, 31, 66-69 30, 70] Therefore, we used the SSDP program developed by Krissnel and Agmon,[71] for a correct analysis of the data based on the GR model. The values of the rate constants for the proton-transfer, k_{PT} (10 ns^{-1}), and recombination, k_{rec} (6 Å/ns) obtained here (Table 3), are equal to the ones reported in a previous work.[38]

We now study the emission decays of HPTS in a DCM suspension in presence of ~1% water (Figure 4). In order to verify the validity of the GR model for this system, the emission decays were firstly fitted to a multiexponential function (Figure S7B, in ESI†). In similarity with HPTS in bulk water, a multiexponential behaviour is observed, and three components of 60 ps, 500 ps and 3.5 ns, are required at the blue part of the spectrum to get a good fit (χ^2 = 1.180) (Figure S7B and Table 2). This behaviour indicates that for HPTS in water microdroplets in a DCM suspension, the geminate recombination is also present. Thus, we analysed the emission decays applying the reversible diffusion-assisted GR model (SSDP program) (Figure 6A).[71] For a correct determination of k_{PT} and k_{rec}, we also took into account the diffusion coefficient of the ion-pair (RO^-*---H_3O^+) in the microdroplet (more details about the GR model in ESI†). Previous studies in reverse micelles showed that the diffusion coefficients (D) obtained were smaller when the micelle size decreases.[33] However, as we did not estimate the size of the microdroplet, we assume that D value is similar to that in the bulk water (9.5 x 10^{-5} cm^2/s^1).[38] With the parameters described in ESI†; the D, the contact distance minimum (a = 6.8 Å), the dimensionality (d = 3), the Debye radius (R_D=28 Å) and the RO^-* lifetime (τ_f = 3.5 ns); obtained from the previous multiexponential fit, we calculated k_{PT} and k_{rec} using the GR model. The obtained values for both constants are k_{PT} = 13 ns^{-1} and k_{rec} = 7.5 Å/ns, respectively (Table 3, Scheme 2). These values are higher than those obtained in bulk water (k_{PT} = 10 ns^{-1} and k_{rec} = 6 Å/ns). This is due to the reduced size of the reaction sphere allowing a faster proton transfer and increase in the probability of return of the proton from the water-DCM boundary, as it cannot diffuse in the hydrophobic DCM environments. Within the water microdroplets, the

solvation and hydration will be affected thus giving rise to faster PT reaction. It has been shown that the recombination process of HPTS trapped with reverse micelle becomes faster for small micelle sizes, as a result of closer ion-pair parts.[33]

3.2.2.2 HPTS/MCM-41 in DCM suspension containing water

Here, we focus on the effect of water on the emission decay of the HPTS/MCM-41 complexes in DCM suspensions. Figure 4 shows the results using a sample containing 0.6% of water. The signal were initially fitted to a multiexponential function with time constants of: 200 ps (present as a decay and rise in the blue and red parts of the emission spectrum, respectively), 1.2 and 4.5 ns (Figure S7C and Table 2). The multiexponential behaviour of the decays indicates the presence of a GR process in this system as well. Furthermore, the time-resolved emission spectra (TRES) (Figure 5) also suggest the presence of the recombination process as the 440 nm-band corresponding to the emission of the protonated form giving place to the 515 nm emission band, does not disappear entirely at longer delay times (7 and 12 ns). This observation clearly reflects the reversible ESPT reaction nature of HPTS/MCM-41 in presence of water.

Thus, we analysed the data using the GR model. Figure 6B shows the experimental TCSPC signals of ROH* and RO^-* interacting with MCM41 in DCM suspensions containing water along with the obtained fits from GR model. Table 3 shows the values of the fitting parameters. For the analysis and based on the consideration given in ESI†, we assumed the following: i) the Debye radius (Eq. 1.2 in ESI†), which depends on the negative and positive charges (total z = 4), is equal to that in bulk water, although in this case the interaction with the surface of the MCM-41 may produce a partial loss of charge; ii) the proton diffusion coefficient (D) near the MCM-41 surface (assumed similar to that of water confined within the mesoporous material (2.4×10^{-5} cm^2/s)[72, 73]), is different from that in bulk water. iii) the proton transferred near the silica surface can hop in a two-dimensional space (*d=2)* different from the bulk water scenario where it is diffusing in three dimensions.[38]

The obtained values of k_{PT} (5.4 ns^{-1}) and k_{rec} (2.2 Å/ns) for HPTS adsorbed on MCM-41 differ significantly from the ones without interactions with MCM41 (13 ns^{-1} and 7.5 Å/ns, respectively). The slowing down of the ESPT reaction rate constants in MCM-41 can be explained by a loss in the photoacidity of the dye. When HPTS

interacts through its sulfonate groups (SO_3^-) with the OH ones of the MCM-41 surface, a partial loss of the negative electronic charge of SO_3^- is generated. This loss of charge provokes a decrease in the photoacidity of HPTS molecule. Furthermore, the recombination processes is also slower, which could be a result of the immobility of RO^- on the silica-framework. In this scenario, only the proton diffusion is taking place to the surrounding water molecules of the droplet or layer, while this process in the DCM containing water is assisted by the mutual diffusion of both RO^- and H_3O^+.

Figure S8 (ESI†) shows a comparison of the time-resolved emission signals of the ROH* form of HPTS and HPTS/MCM-41 in DCM suspensions containing water, in linear and logarithmic scales. The contribution of the initial short-time component, associated with the ESPT process is larger when HPTS is interacting with MCM-41. This is in agreement with the obtained k_{PT} values for HPTS and HPTS/ MCM-41 in DCM containing water (5.4 and 13 ns^{-1}, respectively). The amplitude of the long-time fluorescence tail is also higher in the case of HPTS/MCM-41. This can be explained by the difference in the dimensionality of the proton diffusion space of the two samples (d = 2 in HPTS/MCM-41 and d = 3 in HPTS without MCM-41). When the proton is transferred near the MCM41 surface, it is hopping in a two-dimensional space (d = 2), leading to an increases in the probability of the GR process.[38, 39]

3.2.2.3 HPTS/MCM-41 in DCM suspension containing deuterated water

The rate of the ESPT process of HPTS in D_2O is distinguishably slower than in H_2O.[74] The kinetic isotope effect (KIE) for HPTS in bulk water is ~ 3.[74] Thus, we examined the KIE on the ESPT reaction in the HPTS/MCM-41 hybrid complexes by adding 20 μL of D_2O to 10 mg/ml of HPTS/MCM-41 in a DCM suspension. The steady-state absorption and emission spectra are similar to those obtained for HPTS/MCM-41 with H_2O (Figure S9A in ESI†), which indicates the same photobehaviour with the anion formation. Figure S9B (ESI†) displays representative emission decays in presence of H_2O and D_2O observed at 550 and upon excitation at 370 nm, and Table 2 gives the relevant values from the multiexponential fits. As in the case of H_2O, using D_2O three exponentials are required to get an accurate fit giving time constants of 350 ps, 980 ps and 5.1 ns. To further elucidate the deuterion transfer reaction dynamics, the TCSPC signals were fitted using the GR model.[71] Taking into account the above assumptions of locating HPTS on MCM41 surface and the supposed

diffusion coefficient (more details in ESI†) of the deuterated water on mesoporous material (D_{deut} = 1.5 x 10^{-5} cm^2/s), the obtained SSDP fit is of good quality at both wavelengths of the observation (Figure 6C). The values of k_{PT} and k_{rec} are 2.7 ns^{-1} and 1.7 Å/ns, respectively (Table 3). For the proton transfer process, the KIE k^H_{PT}/k^D_{PT} = 2, which is larger than the normal one (1.4), while for the recombination event, k^H_{rec}/k^D_{rec} = is 1.3. Our result is in agreement with the results observed in bulk water where the KIE in the proton transfer reaction was 3.[25, 31, 64, 75] The difference with the bulk water might be result of a combined effects of a strong interaction between HPTS and MCM41 framework and the restricted diffusion space of adsorbed HPTS, provided by the water microdroplet. On the other hand, changes in the dipole moments orientation of the surrounding water molecules due to the interactions with the MCM-41 surface could alter its H-bond network and thus the proton transfer rate constants.

The above results demonstrate that the interaction with the MCM-41 surface modifies the HPTS photoreaction as the ESPT dynamics in presence of water is different from that in bulk water. A different behaviour was observed in previous studies where HPTS is interacting with alumina and silica surfaces.[38, 39] A proton-transfer dynamics similar to that in bulk water was reported.[38] Another example was the study of HPTS in hydrated porous silicon (PSi).[39] The forward ESPT reaction was slightly faster (90 ps) than the observed in bulk water (105 ps), while that of the recombination process was not different from the bulk one.[39] To obtain information in the ultrashort regime, we performed fs-experiments.

3.3 Femtosecond Time-Resolved Fluorescence Observation

The ultrafast behaviours of HPTS/MCM-41 in DCM suspensions and upon addition of 20 μL of water were studied. Exciting at 370 nm, the molecular system is brought to S_1 almost without excess of vibrational energy. Figures 7 and 8 show the fluorescence transients of HPTS/MCM-41 in DCM suspensions without and in presence of water, at the indicated emission wavelengths. Table 4 gives the results of the multiexponential fits, taking into account the long ps-components discussed in the previous sections.

Firstly, we analyse the ultrafast behaviour of HPTS/MCM-41 in DCM suspensions. We used three components in a multiexponential fit of the data. The time constants are: 100-120 fs, 1.8-2.0 ps and 350 ps. The latter is fixed in the fit taking into account the result obtained from the TCSPC measurements (Table 2). All the components appear as decays at all wavelengths of observation. Since the steady-state and TCSPC results do not show any evidence of ESPT, we assign the fs-component to intramolecular vibrational-energy redistribution (IVR), while the fast one (1.8-2 ps) is due to a combination of the vibrational cooling (VC) and charge transfer (CT) processes in the excited ROH form (Scheme 3). Organic molecules with sizes comparable to HPTS, such as 2'(2-hydroxyphenyl)-benzothiazole (HBT) and 1,8-dihydroxy-9,10-anthraquinone (DHAQ), for example, show vibrational relaxation times similar to the obtained here.[76-79]

The ultrafast dynamics of HPTS/MCM-41 complexes in a DCM suspension containing 1% of water were examined. Four exponential components were needed to accurately fit the transient, giving times of ~0.8 ps, ~5 ps, 200 ps and 4.5 ns (Table 4). The longest component is fixed in the fit using the value obtained in the ps-ns experiments. The ultrafast component (~0.8 ps) is decaying at 410 (44 %) to 430 nm (19%), and rising from 450 to 500 nm. The 5 and 200-ps components are decaying up to 500 nm, and are rising from 550 nm observation. According to the obtained results in the picosecond part, the 200-ps time constant is due to the ESPT process which takes place between the water molecules and HPTS absorbed on the surface of the mesoporous materials. In similarity with previous studies on the ultrafast dynamics of HPTS,[37, 80] we assign the ultrafast component (~0.8 ps) to solvation dynamics of the locally excited (LE) state of ROH*. A previous study of HPTS shown its charge redistribution upon excitation, leading to a change in its dipole moment.[81] Thus, we suggest that the LE undergoes an interconversion giving place to a charge transfer (CT) intermediate in 5 ps (Scheme 3). This process is assisted by the solvent in agreement with previous studies.[28, 32, 37, 82] Here HPTS is complexed to MCM-41 external surface, and is surrounded by a water shell, which in turn is within a DCM solution. It should be noted that vibrational cooling (VC) in these systems occurs on comparable time scales and thus this component most probably represents a combination of both CT and VC processes. A similar behaviour of HPTS confined in γ-CD was reported, where the observed time constants were 800 fs and 8 ps.[37] These constants are slower than those obtained in bulk water (300 fs and 3 ps, respectively).[18, 28, 29, 32, 64] Numerous studies

have shown that the mobility of the adsorbed and/or confined water is hindered due to its interactions with the polar groups of the host system.[83-86] This restriction affects the polarity and the dielectric constant of the adsorbed/confined water, which produces a slowing down of the solvation dynamics.[83-90] As example, it is well known that adsorbed water molecules on biological or chemical hosts (micelles, cyclodextrins, proteins and silica-based materials) have much slower dynamics than of the bulk one.[91-94] On the other hand, the interaction of HPTS with the MCM-41 surface influences the electronic distribution of the dye, affecting thus the LE→CT conversion time. Molecules as Nile Red, 2-(2'-hydroxyphenyl) benzazoles (HBT, HBO), Sudan I, 7-hydroxyquinolein (7-HQ), Salicylaldehyde azine (SAA) interacting with MCM-41 and faujasite zeolites show that the involved interactions, slow down the solvation and involved photophysical processes.[4, 6, 7, 95, 96] Therefore, compared to the pure water scenario the increase of both time constants (~0.8 ps and 5 ps) is due to i) the nature of adsorbed water on MCM-41, ii) the electrostatic interactions between HPTS and the surface of MCM-41, and iii) the decrease of freedom of solvent motion and HPTS molecules adsorbed on the surface. Scheme 3 summarizes the above discussion.

4. Conclusion

In this work, we have presented studies on the ground and excited state interaction of HPTS with and without MCM-41 in solid-state and in DCM suspensions, in absence and in presence of small amount of water. In the solid-state, HPTS exhibits aggregates formation as result of π-π interactions. These aggregates, formed by the protonated species (ROH), show broad absorption and emission bands and multiexponential emission decays. The adsorption of HPTS on MCM-41 produces a blue-shift in its emission spectrum and a change in the ps-dynamics, as result of a decrease in the aggregates population and an increase in the population of ROH monomers. Experiments using silica particles and concentration effect suggest that HPTS interacts with the MCM-41 surface. In presence of water, HPTS exhibits an excited-state proton transfer (ESPT) reaction producing an excited deprotonated form (RO^-*). In the global mechanism, the geminate recombination (GR) process occurs, and the emission decays are fitted using the GR model. For HPTS in DCM suspensions containing water, the obtained values of the proton-transfer rate constant k_{PT} (13 ns^{-1}), and of the recombination k_{rec} (7.5 Å/ns) are higher than those in pure water (k_{PT} = 10 ns^-

[1] and k_{rec} = 6 Å/ns) due to the reduced size of the reaction sphere in the former case. However, for the HPTS/MCM-41 complexes a slowing down of the proton transfer and recombination processes (k_{PT} = 5.4 ns^{-1} and k_{rec} = 2.2 Å/ns) are observed due to a decrease in the HPTS photoacidity nature and the reduction of the diffusion space of adsorbed HPTS and water molecules. The KIE for the recombination process (k^H_{rec}/k^D_{rec}) is 1.3, while for the proton transfer one (k^H_{PT}/k^D_{PT}) is 2. This latter is larger than the normal KIE (1.4) but lower than the one observed for the ESPT reaction in bulk water (~3). Finally, the fs-study of HPTS/MCM-41 complexes without and with water shows two components; having time constants of ~120 fs and ~0.8 ps, respectively, assigned to IVR; and another longer one of ~2 and 5 ps, respectively, due to a combination of the VC and CT processes of the ROH* form. Our results bring new findings on the proton-transfer dynamics of HPTS adsorbed in mesoporous materials. They can be used in the design of electro-optic devices based on the phoacidity of HPTS and silica-based materials.

Acknowledgments

This work was supported by the MINECO and JCCM through projects: Consolider Ingenio 2010 (CSD2009-0050, MULTICAT), MAT2011-25472, MAT2014-57646-P and PEII-2014-003-P.

Electronic Supplementary Information (ESI†) available: Figure S1 shows the excitation and absorption spectra of (A) HPTS and (B) HPTS/MCM-41 in solid-state. Figure S2 exhibits UV-visible absorption, emission and excitation spectra of HPTS and HPTS/MCM-41 in DCM suspensions. Figure S3 presents UV-visible absorption, emission spectra, and magic-angle emission decays of HPTS/SiO_2 in a DCM suspension. Figure S4 shows UV-visible absorption and emission spectra of HPTS in DCM suspensions and in presence of different amounts of water. Figure S5 shows UV-visible absorption and emission spectra of HPTS/MCM-41 (hydrated) in DCM suspensions. Figure S6 exibits UV-visible absorption and emission spectra, and magic-angle emission decays of HPTS (10^{-3} M) interacting with MCM-41 in DCM suspensions. Figures S7 and S8 show the magic-angle emission decays of HPTS in presence of water analyzed from multiexponential function and GR model, respectively. Figure S9 presents UV-visible absorption and emission spectra, and magic-angle

emission decays of HPTS/MCM-41 in DCM suspensions containing 1% of deuterated water. Table S1 shows the values of time constants of HPTS, HPTS (10^{-3} M)/MCM-41 and HPTS (10^{-5} M)/SiO_2 in DCM suspensions. Finally, an explanation of the reversible diffusion model is added. See DOI: XXXX

References

1. A. Krysztafkiewicz, S. Binkowski and T. Jesionowski, *Appl. Surf. Sci.*, 2002, **199**, 31-39.
2. S. K. Parida, S. Dash, S. Patel and B. K. Mishra, *Adv. Colloid Interface Sci.*, 2006, **121**, 77-110.
3. F. Goettmann and C. Sanchez, *J. Mater. Chem.*, 2007, **17**, 24-30.
4. B. Cohen, S. Wang, J. A. Organero, L. F. Campo, F. Sanchez and A. Douhal, *J. Phys. Chem. C*, 2010, **114**, 6281-6289.
5. Z. Wu and D. Y. Zhao, *Chem. Commun.*, 2011, **47**, 3332-3338.
6. M. Gil, C. Martin and A. Douhal, *J. Phys. Chem. C*, 2011, **115**, 14687-14697.
7. N. Alarcos, B. Cohen and A. Douhal, *J. Phys. Chem. C*, 2014, **118**, 19431-19443.
8. C. Martín, P. Piatkowski, B. Cohen, M. Gil, M. T. Navarro, A. Corma and A. Douhal, *J. Phys. Chem. C*, 2015, **119**, 13283-13296.
9. P. Innocenzi and L. Malfatti, *Chem. Soc. Rev.*, 2013, **42**, 4198-4216.
10. T. Wagner, S. Haffer, C. Weinberger, D. Klaus and M. Tiemann, *Chem. Soc. Rev.*, 2013, **42**, 4036-4053.
11. C. Perego and R. Millini, *Chem. Soc. Rev.*, 2013, **42**, 3956-3976.
12. N. Linares, A. M. Silvestre-Albero, E. Serrano, J. Silvestre-Albero and J. Garcia-Martinez, *Chem. Soc. Rev.*, 2014, **43**, 7681-7717.
13. Z. Tao, *RSC Advances*, 2014, **4**, 18961-18980.
14. A. Taguchi and F. Schüth, *Microporous Mesoporous Mater.*, 2005, **77**, 1-45.
15. R. M. Martín-Aranda and J. Čejka, *Top. Catal.*, 2010, **53**, 141-153.
16. J. F. Ireland and P. A. H. Wyatt, in *Adv. Phys. Org. Chem.*, ed. V. Gold, Academic Press, 1976, vol. Volume 12, pp. 131-221.
17. L. M. Tolbert and K. M. Solntsev, *Acc. Chem. Res.*, 2002, **35**, 19-27.
18. D. B. Spry and M. D. Fayer, *J. Chem.Phys.*, 2008, **128**, 084508.
19. N. Agmon, *J. Phys. Chem. A*, 2005, **109**, 13-35.
20. B. Cohen, D. Huppert and N. Agmon, *J. Phys. Chem. A*, 2001, **105**, 7165-7173.
21. L. G. Arnaut and S. J. Formosinho, *J. Photochem. Photobiol., A*, 1993, **75**, 1-20.
22. O. F. Mohammed, D. Pines, J. Dreyer, E. Pines and E. T. J. Nibbering, *Science*, 2005, **310**, 83-86.
23. O. F. Mohammed, D. Pines, E. Pines and E. T. Nibbering, *Chem. Phys.*, 2007, **341**, 240-257.
24. N. Agmon, D. Huppert, A. Masad and E. Pines, *J. Phys. Chem.*, 1991, **95**, 10407-10413.
25. O. F. Mohammed, J. Dreyer, B. Z. Magnes, E. Pines and E. T. Nibbering, *Chemphyschem*, 2005, **6**, 625-636.
26. O. F. Mohammed, D. Pines, E. T. J. Nibbering and E. Pines, *Angew. Chem. Int. Ed.*, 2007, **46**, 1458-1461.
27. B. J. Siwick, M. J. Cox and H. J. Bakker, *J. Phys. Chem. B*, 2008, **112**, 378-389.
28. T. H. Tran-Thi, T. Gustavsson, C. Prayer, S. Pommeret and J. T. Hynes, *Chem. Phys. Lett.*, 2000, **329**, 421-430.
29. L. Genosar, B. Cohen and D. Huppert, *J. Phys. Chem. A*, 2000, **104**, 6689-6698.
30. M. Smoluchowski, *Z. Phys. Chem.*, 1917, **92**, 129–168.
31. P. Leiderman, L. Genosar and D. Huppert, *J. Phys. Chem. A*, 2005, **109**, 5965-5977.

32. T. H. Tran-Thi, C. Prayer, P. Millié, P. Uznanski and J. T. Hynes, *J. Phys. Chem. A*, 2002, **106**, 2244-2255.
33. B. Cohen, D. Huppert, K. M. Solntsev, Y. Tsfadia, E. Nachliel and M. Gutman, *J. Am. Chem. Soc.*, 2002, **124**, 7539-7547.
34. B. Cohen, C. Martin Álvarez, N. Alarcos Carmona, J. A. Organero and A. Douhal, *J. Phys. Chem. B*, 2011, **115**, 7637-7647.
35. S. Ghosh, S. Dey, U. Mandal, A. Adhikari, S. K. Mondal and K. Bhattacharyya, *J. Phys. Chem. B*, 2007, **111**, 13504-13510.
36. S. K. Mondal, K. Sahu, S. Ghosh, P. Sen and K. Bhattacharyya, *J. Phys. Chem. A*, 2006, **110**, 13646-13652.
37. S. K. Mondal, K. Sahu, P. Sen, D. Roy, S. Ghosh and K. Bhattacharyya, *Chem. Phys. Lett.*, 2005, **412**, 228-234.
38. H. P. Soroka, R. Simkovitch, A. Kosloff, S. Shomer, A. Pevzner, O. Tzang, R. Tirosh, F. Patolsky and D. Huppert, *J. Phys. Chem. C*, 2013, **117**, 25786-25797.
39. T. Hutter, I. Presiado, S. Ruschin and D. Huppert, *Journal of Physical Chemistry C*, 2010, **114**, 2341-2348.
40. J. A. Organero, L. Tormo and A. Douhal, *Chem. Phys. Lett.*, 2002, **363**, 409-414.
41. M. Gil and A. Douhal, *Chem. Phys. Lett.*, 2006, **432**, 106-109.
42. Y. Wang, W. Liu, L. Tang, B. Oscar, F. Han and C. Fang, *J. Phys. Chem. A*, 2013, **117**, 6024-6042.
43. W. Liu, F. Han, C. Smith and C. Fang, *J. Phys. Chem. B*, 2012, **116**, 10535-10550.
44. D. Roy, R. Karmakar, S. K. Mondal, K. Sahu and K. Bhattacharyya, *Chem. Phys. Lett.*, 2004, **399**, 147-151.
45. A. K. Dutta, T. N. Misra and A. J. Pal, *Langmuir*, 1996, **12**, 459-465.
46. M. G. Ivan and J. C. Scaiano, *Chem. Mater.*, 2009, **21**, 3933-3940.
47. Y. Mizobe, M. Miyata, I. Hisaki, Y. Hasegawa and N. Tohnai, *Org. Lett.*, 2006, **8**, 4295-4298.
48. T. Hinoue, Y. Shigenoi, M. Sugino, Y. Mizobe, I. Hisaki, M. Miyata and N. Tohnai, *Chem. Eur. J.*, 2012, **18**, 4634-4643.
49. A. Thomas, S. Polarz and M. Antonietti, *J. Phys. Chem. B*, 2003, **107**, 5081-5087.
50. R. Gepshtein, P. Leiderman, D. Huppert, E. Project, E. Nachliel and M. Gutman, *J. Phys. Chem. B*, 2006, **110**, 26354-26364.
51. T. Mondal, A. K. Das, D. K. Sasmal and K. Bhattacharyya, *J. Phys. Chem. B*, 2010, **114**, 13136-13142.
52. R. Mancinelli, S. Imberti, A. K. Soper, K. H. Liu, C. Y. Mou, F. Bruni and M. A. Ricci, *J. Phys. Chem. B*, 2009, **113**, 16169-16177.
53. S. Gamsey, A. Miller, M. M. Olmstead, C. M. Beavers, L. C. Hirayama, S. Pradhan, R. A. Wessling and B. Singaram, *J. Am. Chem. Soc.*, 2007, **129**, 1278-1286.
54. X.-B. Wang, A. P. Sergeeva, X.-P. Xing, M. Massaouti, T. Karpuschkin, O. Hampe, A. I. Boldyrev, M. M. Kappes and L.-S. Wang, *J. Am. Chem. Soc.*, 2009, **131**, 9836-9842.
55. M. Gil, J. A. Organero, E. Peris, H. García and A. Douhal, *Chem. Phys. Lett.*, 2009, **474**, 325-330.
56. M. Gil, C. Martin, J. A. Organero, M. T. Navarro, A. Corma and A. Douhal, *J. Phys. Chem. C*, 2010, **114**, 6311-6317.

57. N. Sarkar, K. Das, D. N. Nath and K. Bhattacharyya, *Langmuir*, 1994, **10**, 326-329.
58. J. Sivaguru, A. Natarajan, L. S. Kaanumalle, J. Shailaja, S. Uppili, A. Joy and V. Ramamurthy, *Acc. Chem. Res.*, 2003, **36**, 509-521.
59. A. P. Penner, W. Siebrand and M. Z. Zgierski, *J. Chem.Phys.*, 1978, **69**, 5496-5508.
60. M. R. di Nunzio, B. Cohen, S. Pandey, S. Hayse, G. Piani and A. Douhal, *J. Phys. Chem. C*, 2014, **118**, 11365-11376.
61. B. Cohen, D. Huppert and N. Agmon, *J. Am. Chem. Soc.*, 2000, **122**, 9838-9839.
62. M. Rini, D. Pines, B.-Z. Magnes, E. Pines and E. T. J. Nibbering, *J. Chem.Phys.*, 2004, **121**, 9593-9610.
63. K. M. Solntsev, D. Huppert and N. Agmon, *J. Phys. Chem. A*, 2001, **105**, 5868-5876.
64. D. B. Spry, A. Goun and M. D. Fayer, *J. Phys. Chem. A*, 2007, **111**, 230-237.
65. B. J. Siwick and H. J. Bakker, *J. Am. Chem. Soc.*, 2007, **129**, 13412-13420.
66. E. Pines and D. Huppert, *Chem. Phys. Lett.*, 1985, **116**, 295-301.
67. N. Agmon, E. Pines and D. Huppert, *J. Chem.Phys.*, 1988, **88**, 5631-5638.
68. E. Pines and D. Huppert, *J. Am. Chem. Soc.*, 1989, **111**, 4096-4097.
69. D. Huppert, S. Y. Goldberg, A. Masad and N. Agmon, *Phys. Rev. Lett.*, 1992, **68**, 3932-3935.
70. D. P., *J. Electrochem. Soc.*, 1942, **82**, 265.
71. E. B. Krissinel and N. Agmon, *J. Comput. Chem.*, 1996, **17**, 1085-1098.
72. I. M. Briman, D. Rébiscoul, O. Diat, J. M. Zanotti, P. Jollivet, P. Barboux and S. Gin, *J. Phys. Chem. C*, 2012, **116**, 7021-7028.
73. A. A. Milischuk and B. M. Ladanyi, *J. Chem.Phys.*, 2011, **135**, 174709.
74. P. Ehud, in *Isotope Effects In Chemistry and Biology*, CRC Press, 2005, pp. 451-464.
75. M. Rini, B.-Z. Magnes, E. Pines and E. T. J. Nibbering, *Science*, 2003, **301**, 349-352.
76. M. Rini, J. Dreyer, E. T. J. Nibbering and T. Elsaesser, *Chem. Phys. Lett.*, 2003, **374**, 13-19.
77. M. Rini, A. Kummrow, J. Dreyer, E. T. J. Nibbering and T. Elsaesser, *Faraday Discuss.*, 2003, **122**, 27-40.
78. J. R. Choi, S. C. Jeoung and D. W. Cho, *Chem. Phys. Lett.*, 2004, **385**, 384-388.
79. O. F. Mohammed, D. Xiao, V. S. Batista and E. T. J. Nibbering, *J. Phys. Chem. A*, 2014, **118**, 3090-3099.
80. B. Cohen, C. M. Alvarez, N. A. Carmona, J. A. Organero and A. Douhal, *Phys. Chem. Chem. Phys.*, 2011, **13**, 1819-1826.
81. L. N. Silverman, D. Spry, S. G. Boxer and M. Fayer, *J. Phys. Chem. A*, 2008, **112**, 10244-10249.
82. S. Mondal, S. Ghosh, K. Sahu, P. Sen and K. Bhattacharyya, *J Chem Sci*, 2007, **119**, 71-76.
83. B. Bagchi, *Chem. Rev.*, 2005, **105**, 3197-3219.
84. S. K. Pal, J. Peon, B. Bagchi and A. H. Zewail, *J. Phys. Chem. B*, 2002, **106**, 12376-12395.
85. N. Nandi, K. Bhattacharyya and B. Bagchi, *Chem. Rev.*, 2000, **100**, 2013-2046.
86. M. D. Fayer and N. E. Levinger, *Annu. Rev. Anal. Chem.*, 2010, **3**, 89-107.
87. W. H. Thompson, *J. Chem.Phys.*, 2002, **117**, 6618-6628.
88. M. S. Sansom, I. D. Kerr, J. Breed and R. Sankararamakrishnan, *Biophys. J.*, 1996, **70**, 693-702.

89. S. Das, A. Datta and K. Bhattacharyya, *J. Phys. Chem. A*, 1997, **101**, 3299-3304.
90. A. Datta, D. Mandal, S. K. Pal and K. Bhattacharyya, *J. Phys. Chem. B*, 1997, **101**, 10221-10225.
91. A. Douhal, *Chem. Rev.*, 2004, **104**, 1955-1976.
92. S. K. Pal and A. H. Zewail, *Chem. Rev.*, 2004, **104**, 2099-2124.
93. S. Balasubramanian and B. Bagchi, *J. Phys. Chem. B*, 2002, **106**, 3668-3672.
94. R. A. Farrer and J. T. Fourkas, *Acc. Chem. Res.*, 2003, **36**, 605-612.
95. M. Gil, S. Wang, J. A. Organero, L. Teruel, H. Garcia and A. Douhal, *J. Phys. Chem. C*, 2009, **113**, 11614-11622.
96. M. Gil, M. Ziolek, J. A. Organero and A. Douhal, *J. Phys. Chem. C*, 2010, **114**, 9554-9562.

Caption of figures, schemes and tables.

Scheme 1. A) Molecular structures of protonated (ROH) and deprotonated (RO^-) 8-hydroxypyrene-1,3,6-trisulfonate (HPTS). B) General scheme of reversible excited-state intermolecular proton transfer (ESPT) process in excited HPTS considering the geminate recombination process.

Scheme 2. Schematic illustration (not in scale) of A) HPTS and HPTS/MCM-41 in a DCM suspension (brown colour) and B) HPTS trapped within a water droplet in a DCM suspension, and adsorbed on MCM41 surface. We indicate the values of the wavelengths corresponding to the emission intensity maxima and the fluorescence lifetimes (τ_{ROH}, τ_{RO}-) of the formed species. For (B), the values of proton transfer (k_{PT}) and recombination rate (k_{rec}) constants, are also indicated.

Scheme 3. Schematic representation (not in scale) of the observed dynamics of A) HPTS/MCM-41 in a DCM suspension, and B) the same sample as in (A) but containing 1% of water. We show the values of the characteristic parameters.

Table 1. Values of time constants (τ_i), normalized (to 100) pre-exponential factors (a_i) and fractional contributions ($c_i = \tau_i a_i$) obtained from the fit of the emission ps-ns decays of (A) solid HPTS, and (B) solid HPTS/MCM-41 and in DCM suspensions, upon excitation at 350 nm and observation as indicated. The estimated errors for the obtained values are 15-20 %.

Table 2. Values of time constants (τ_i), normalized (to 100) pre-exponential factors (a_i) and fractional contributions ($c_i = \tau_i a_i$) obtained from the fit of the emission ps-ns decays of the indicated samples, upon excitation at 370 nm and observation as indicated. The negative sign for a_1 (c_1) indicates a rising component in the emission signal. The estimated errors for the obtained values are 15-20 %.

Table 3. Kinetic parameters for the proton-transfer reaction using the geminate recombination (GR) model. k_{PT} and k_{rec} are the rate constants of forward and backward (proton transfer and recombination reactions) whose values are obtained from the fit of the experimental data using the reversible proton transfer model (see text). "R_D" is the debye radius, "a" the minimum contact distance, "d" the number of dimensions in the diffusion space, "D" the coefficient diffusion and "τ_f" the excited-state lifetime of the RO^-.

Table 4. Values of time constants (τ_i) and normalized (to 100) pre-exponential factors (a_i) of the functions used to fit the fs-emission transients of HPTS/MCM-41in DCM suspensions with and without water, upon excitation at 350 nm and observation as indicated. (*) Fixed value in the fit taken as a mean lifetime from the TCSPC experiments. The negative sign for a_i indicates a rising component in the emission signal. The estimated errors for the obtained values are 15-20 %.

Figure 1. Normalized (to the maximum intensity) Uv-visible diffuse transmittance and fluorescence spectra of HPTS (solid line) and HPTS/MCM-41 (dashed line) in solid-state. For emission, the excited wavelength was 350 nm. F(R) is the Kubelka-Munk function. F(R)=((1-R)2)/2R, where R is the diffuse reflectance from the sample.

Figure 2. Normalized Uv-visible diffuse transmittance and fluorescence spectra of HPTS/MCM-41in DCM suspension (solid line) and upon addition of 20 μL of water to 3 ml of the previous solution (dashed line). For emission, the excited wavelength was 370 nm. F(R) is the Kubelka-Munk function. F(R)=((1-R)2)/2R, where R is the diffuse reflectance from the sample.

Figure 3. Magic-angle emission decays of (1) solid HPTS and (2) solid HPTS/MCM-41 and (3) HPTS/MCM-41 in DCM suspension, observing at (A) 450 nm and (B) 500 nm. The samples were excited at 350 nm. The solid lines are from the best-fit using a multiexponential function. IRF is the instrumental response function (≈ 40 ps).

Figure 4. Magic-angle emission decays of (1) HPTS in bulk water (pH ≈ 6.2), and (2) HPTS and (3) HPTS/MCM-41 in DCM suspensions in presence of 20 μL of water in 3 ml of DCM solution. Figure B is a zoom of figure A. The samples were excited at 370 nm and observed at 550 nm. The solid lines are from the best-fit using tri-exponential function.

Figure 5. Normalized (to the maximum of intensity) magic-angle time-resolved emission spectra (TRES) of HPTS/MCM-41 in DCM suspension containing 1% of water and gated at the indicated delay times after excitation at 370 nm.

Figure 6. Magic-angle emission decays of A) HPTS in DCM suspension in presence of water, B) HPTS/MCM-41 in DCM suspension containing water, and C) with deuterium oxide. The samples were excited at 370 nm and observed at 430 and 550 nm. The solid lines are obtained from the computer fit using the GR model.

Figure 7. Representative fs-emission transients of HPTS/MCM-41 in DCM suspensions, upon excitation at 370 nm and gating as indicated. The solid lines are from the best multiexponential fits and IRF is the instrumental response function (~ 220 fs).

Figure 8. (A) Representative fs-emission transients of HPTS/MCM-41 in DCM suspensions upon addition of water (20 μL to 3 ml of DCM). (B) is a zoom of (A). The samples were excited at 370 nm and the emission gated as indicated in the figure. The solid lines are from the best multiexponential fits.

Scheme 1

A)

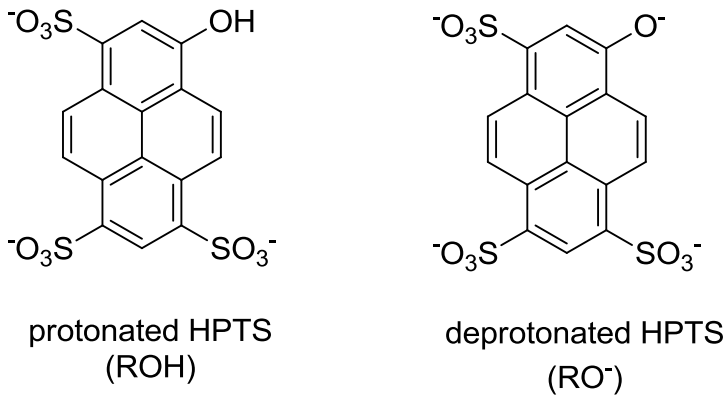

B)

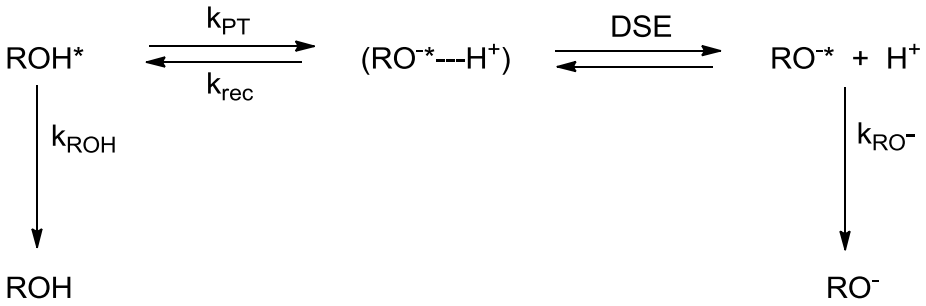

Scheme 2

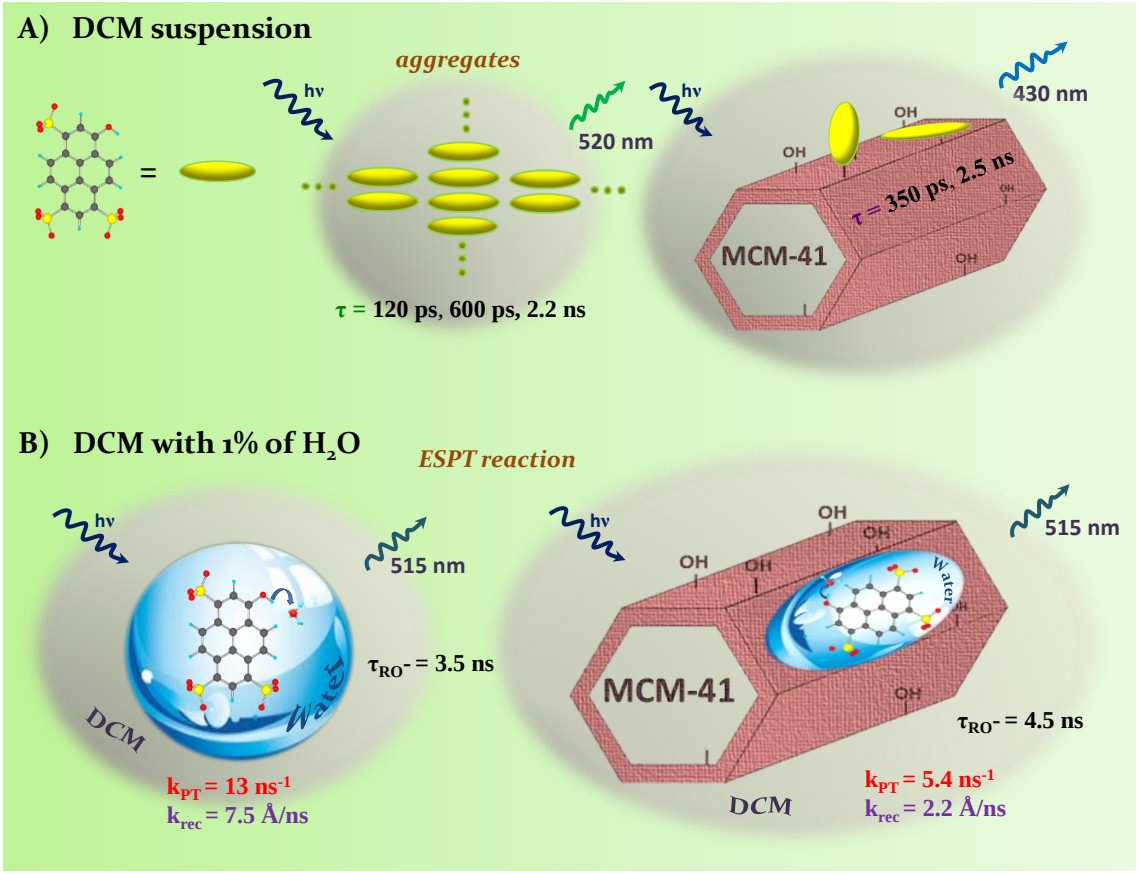

Scheme 3

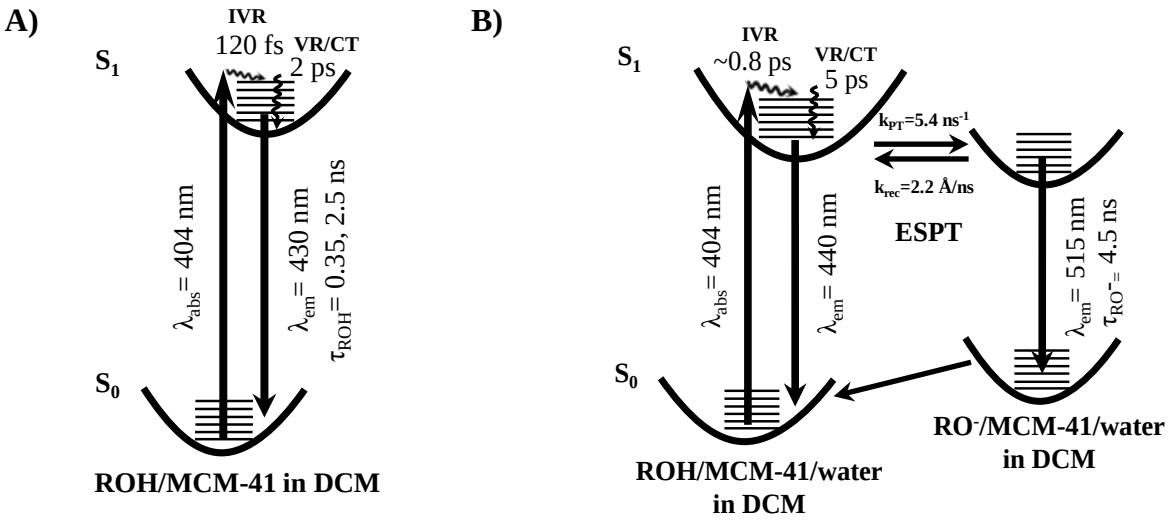

Figure 1

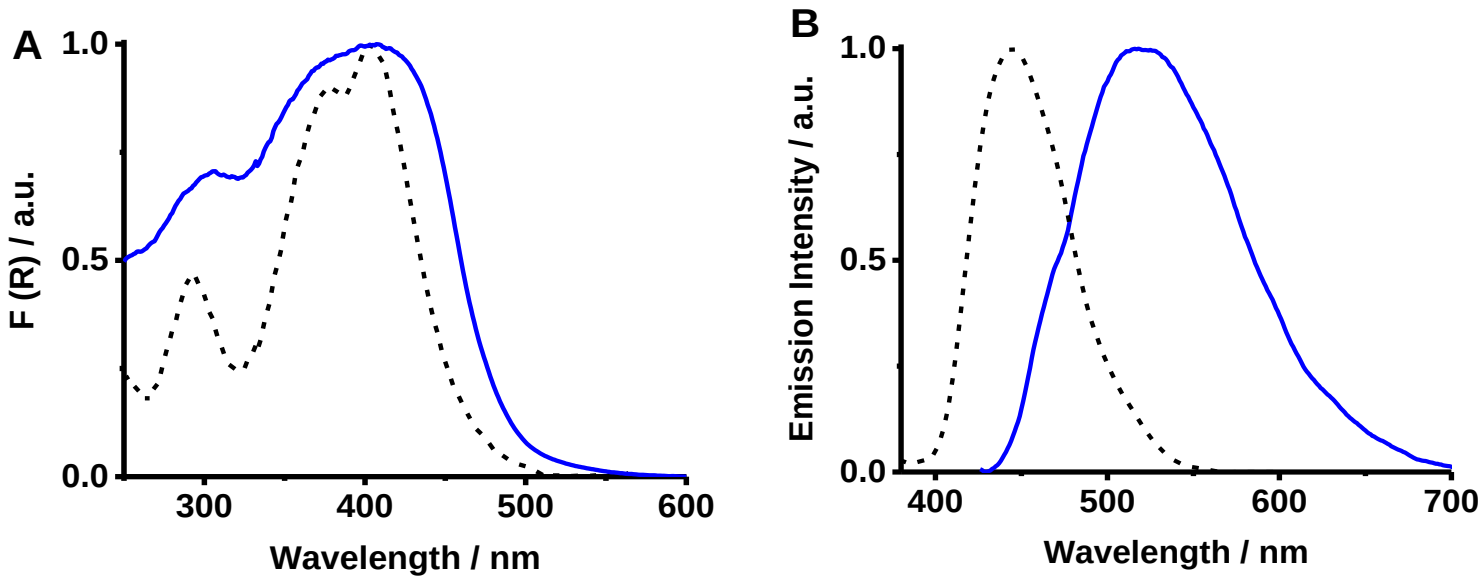

Figure 2

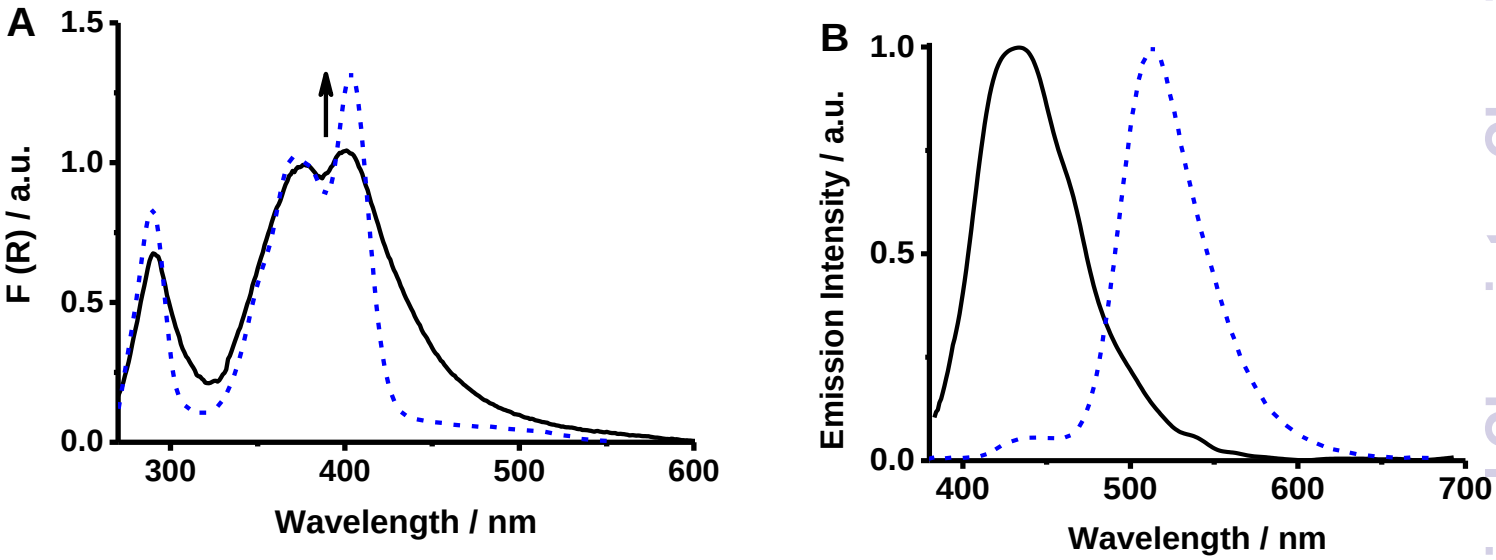

Figure 3

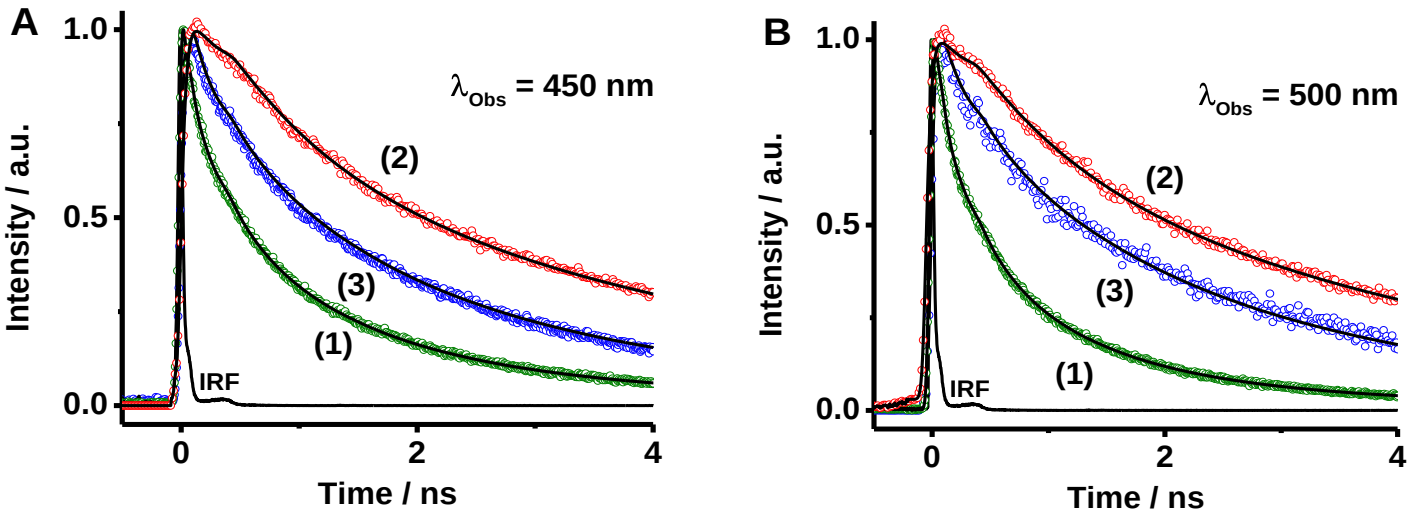

Figure 4

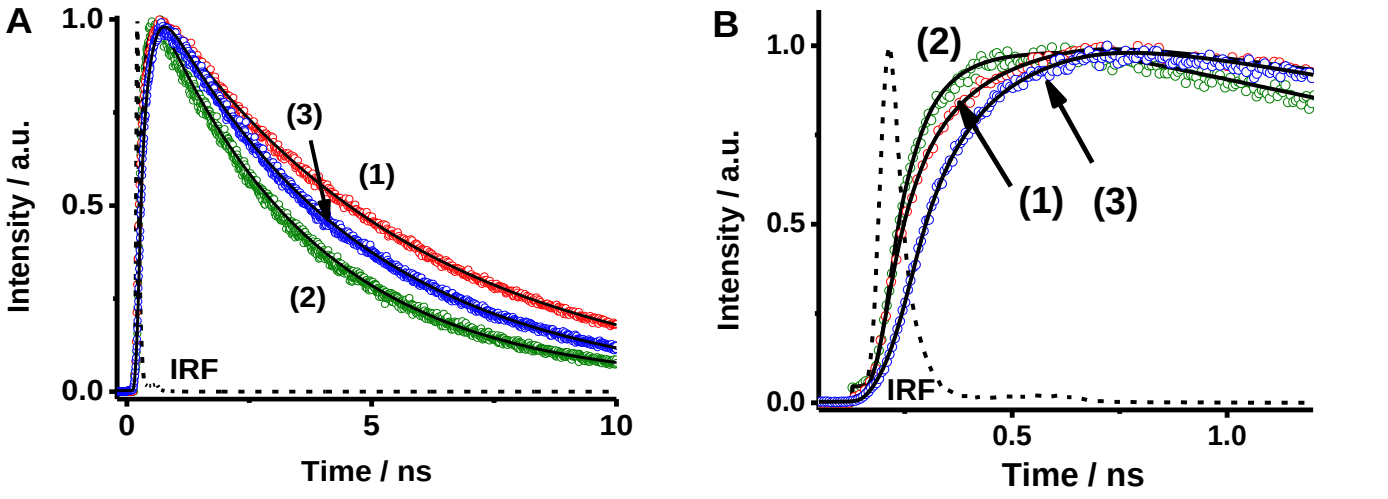

Figure 5

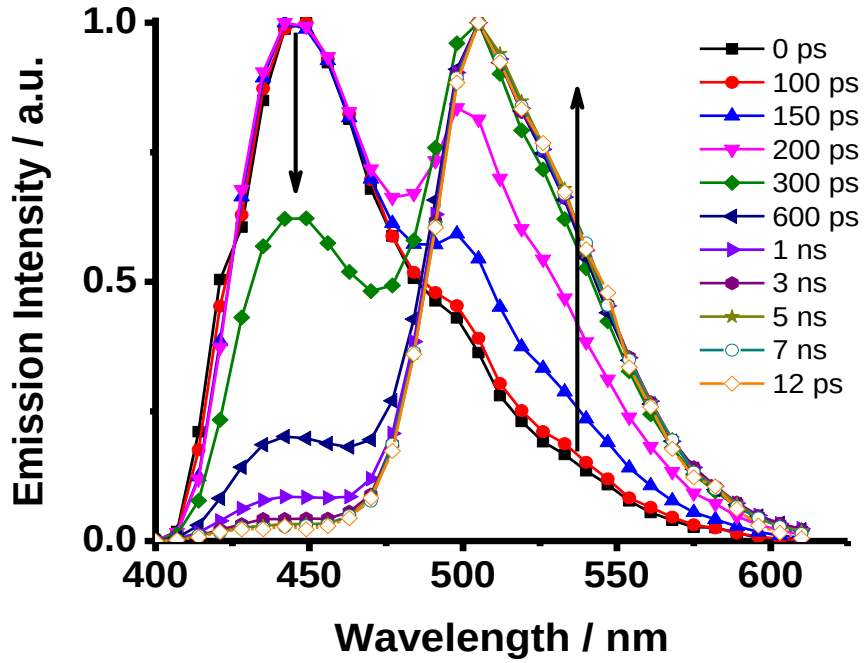

Figure 6

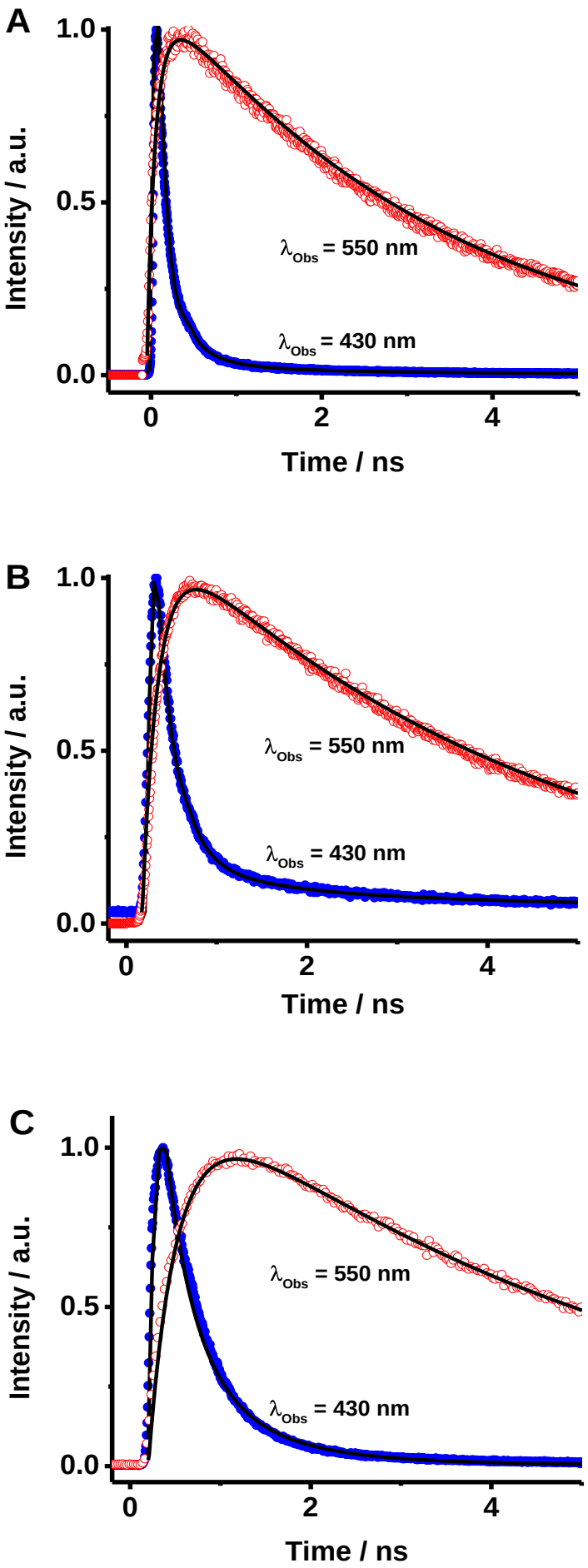

Figure 7

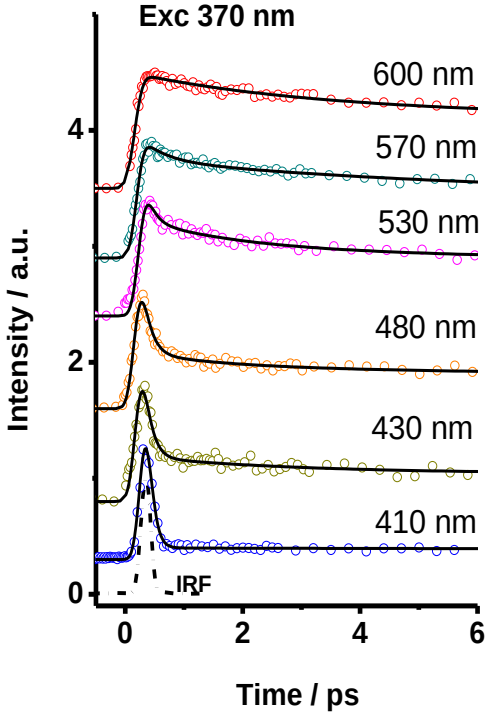

Figure 8

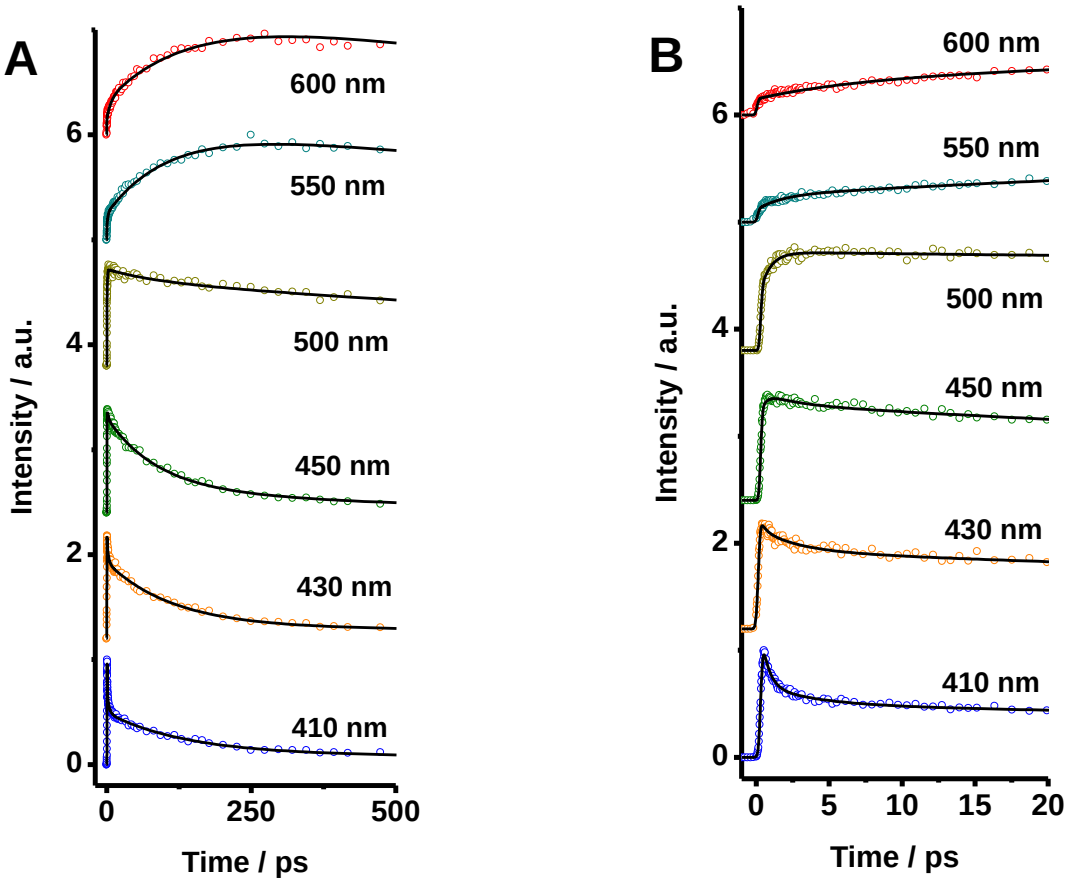

Table 1

A) Sample	λ_{Obs}/nm	τ_1 / ps	a_1 %	c_1 %	τ_2 / ps	a_2 %	c_2 %	τ_3 / ns	a_3 %	c_3 %
	450	**120**	42	5	**600**	36	35	**2.2**	22	60
	470	**120**	43	6	**600**	41	34	**2.2**	16	60
HPTS	490	**120**	47	7	**600**	39	34	**2.2**	14	59
(solid)	510	**120**	53	8	**600**	35	33	**2.2**	12	59
	525	**120**	57	9	**600**	32	32	**2.2**	11	59
	550	**120**	60	10	**600**	28	30	**2.2**	12	60
	575	**120**	63	11	**600**	25	28	**2.2**	12	61
	600	**120**	65	12	**600**	22	23	**2.2**	13	65

B) Sample	λ_{Obs}/nm	τ_1 / ps	a_1 %	c_1 %	τ_2 / ns	a_2 %	c_2 %
	400	**840**	36	13	**3.9**	64	87
	415	**840**	36	12	**3.9**	64	88
HPTS/MCM-41	440	**840**	35	11	**3.9**	65	89
(solid)	450	**840**	34	11	**3.9**	66	89
	470	**840**	33	9	**3.9**	67	91
	500	**840**	33	9	**3.9**	67	91
HPTS/MCM-41/DCM	400	**350**	48	11	**2.5**	52	89
(suspension)	415	**350**	46	11	**2.5**	54	89
	430	**350**	43	9	**2.5**	57	91
	450	**350**	39	8	**2.5**	62	92
	470	**350**	38	7	**2.5**	62	93
	500	**350**	37	6	**2.5**	63	94

Table 2

Sample	λ_{Obs}/nm	τ_1 / ps	a_1%	c_1%	τ_2 / ns	a_2%	c_2%	τ_3 / ns	a_3%	c_3%
HPTS/H_2O	430	**90**	94	37	**0.72**	6	63	-	-	-
	450	**90**	93	57	**0.72**	6	30	**5.0**	1	13
	475	**90**	81	56	**0.72**	5	31	**5.0**	14	13
	500	**90**	-100	-100	-	-	-	**5.0**	100	100
	550	**90**	-100	-100	-	-	-	**5.0**	100	100
	600	**90**	-100	-100	-	-	-	**5.0**	100	100
HPTS/DCM+H_2O	430	**60**	91	54	**0.50**	8	22	**3.5**	1	24
	450	**60**	86	22	**0.50**	7	8	**3.5**	7	70
	475	**60**	5	1	-	-	-	**3.5**	95	99
	500	**60**	-100	-100	-	-	-	**3.5**	100	100
	550	**60**	-100	-100	-	-	-	**3.5**	100	100
	600	**60**	-100	-100	-	-	-	**3.5**	100	100
HPTS/MCM-41/ DCM+H_2O	430	**200**	91	37	**1.20**	6	22	**4.5**	3	41
	450	**200**	91	34	**1.20**	6	21	**4.5**	3	45
	470	**200**	83	18	**1.20**	6	12	**4.5**	11	70
	500	**200**	-100	-100	**1.20**	3	8	**4.5**	97	92
	550	**200**	-100	-100	-	-	-	**4.5**	100	100
	600	**200**	-100	-100	-	-	-	**4.5**	100	100
HPTS/MCM-41/ DCM+D_2O	430	**350**	85	65	**0.98**	14	22	**5.1**	1	13
	450	**350**	85	65	**0.98**	14	24	**5.1**	1	11
	470	**350**	80	43	**0.98**	14	16	**5.1**	6	41
	500	**350**	-100	-100	-	-	-	**5.1**	100	100
	525	**350**	-100	-100	-	-	-	**5.1**	100	100
	550	**350**	-100	-100	-	-	-	**5.1**	100	100

Table 3

Sample	Dimension	R_D (Å)	a (Å)	k_{PT} (ns^{-1})	k_{REC} (Å/ns)	D (cm^2/s)	τ_f^{-1} (ns^{-1})
HPTS H_2O	3	28.3	6.8	10 ± 0.5	6.0 ± 0.3	9.5×10^{-5}	0.200
HPTS DCM + H_2O	3	28.3	6.8	13 ± 0.6	7.5 ± 0.4	9.5×10^{-5}	0.285
HPTS/MCM-41 + H_2O	2	28.3	6.8	5.4 ± 0.3	2.2 ± 0.2	2.4×10^{-5}	0.220
HPTS/MCM-41 + D_2O	2	28.3	6.8	2.7 ± 0.2	1.7 ± 0.1	1.5×10^{-5}	0.196

Table 4

Sample	λ_{Obs}/nm	τ_1 / fs	a_1%	τ_2 / ps	a_2%	τ_3* / ps	a_3%	τ_4* / ns	a_4%
HPTS/MCM-41	410	**100**	95	**1.8**	2	**350**	3	-	-
	430	**100**	83	**1.8**	7	**350**	10	-	-
	440	**100**	72	**1.8**	12	**350**	16	-	-
	480	**110**	59	**1.8**	18	**350**	23	-	-
	500	**120**	45	**2.0**	27	**350**	28	-	-
	530	**120**	29	**2.0**	35	**350**	36	-	-
HPTS/MCM-41/H_2O	410	**720**	44	**4.6**	14	**200**	42	-	-
	430	**760**	19	**4.8**	13	**200**	68	-	-
	450	**850**	(-)100	**5.0**	12	**200**	68	**4.5**	15
	475	**850**	(-)100	**5.0**	10	**200**	36	**4.5**	54
	500	**850**	(-)100	**5.0**	7	**200**	10	**4.5**	83
	550	-	-	**5.0**	(-)11	**200**	(-)89	**4.5**	100
	600	-	-	**5.0**	(-)8	**200**	(-)92	**4.5**	100

TOC

Photodynamics of HPTS within a water droplet and on hydrated MCM-41 surface.